Jimenez-Rodriguez, M., Monteagudo-Lerma, L., Monroy, E., González-Herráez, M., Naranjo, F.B., 2017, "Widely power-tunable polarization-independent ultrafast mode-locked fiber laser using bulk InN as saturable absorber", Optics Express, 25 (5), pp. 5366-5375.

Available at http://dx.doi.org/10.1364/OE.25.005366

Widely power-tunable polarization-independent ultrafast mode-locked fiber laser using bulk InN as saturable absorber

M. JIMENEZ-RODRIGUEZ,[1,*] L. MONTEAGUDO-LERMA,[1] E. MONROY,[2,3] M. GONZÁLEZ-HERRÁEZ,[1] AND F. B. NARANJO[1]

[1]*Photonics Engineering Group, Electronics Dept (EPS), Alcalá University, 28871, Alcalá de Henares, Madrid, Spain*

[2]*University Grenoble-Alpes, 38000 Grenoble, France.*

[3]*CEA-Grenoble, INAC-PHELIQS, 17 av. des Martyrs 38000 Grenoble, France*

**marco.jimenezr@uah.es*

Abstract: The growing demand of ultrafast mode-locked fiber lasers in the near infrared has boosted the research activity in this area. One of the most convenient ways to achieve passive mode locking consists of inserting a semiconductor saturable absorber in the laser cavity to modulate the losses. However, in such a configuration, the limited power range of operation is still an unsolved issue. Here we report the fabrication of an ultrafast, high-power, widely power-tunable and non-polarization-dependent mode-locked fiber laser operating at 1.55 μm, using an InN layer as saturable absorber. With post-amplification, this laser delivers 55-fs pulses with a repetition rate of 4.84 MHz and peak power in the range of 1 MW in an all-fiber arrangement.

OCIS codes: (060.3510) Lasers, fiber; (140.4050) Mode-locked lasers; (140.7090) Ultrafast lasers; (160.4330) Nonlinear optical materials.

References and links

1. M. E. Fermann, and I. Hartl, "Ultrafast fibre lasers," Nat. Photonics **7**, 868–874 (2013).
2. L. E. Nelson, D. J. Jones, K. Tamura, H. A. Haus, and E. P. Ippen, "Ultrashort-pulse fiber ring lasers," Appl. Phys. B Lasers Opt. **65**, 277–294 (1997).
3. K. Tamura, J. Jacobson, E. P. Ippen, H. A. Haus, and J. G. Fujimoto, "Unidirectional ring resonators for self-starting passively mode-locked lasers," Opt. Lett. **18**, 220–222 (1993).
4. R. J. Mears, L. Reekie, I. M. Jauncey, and D. N. Payne, "Low-noise erbium-doped fibre amplifier operating at 1.54μm," Electron. Lett. **23**, 1026–1028 (1987).
5. M. Jiang, G. Sucha, M. E. Fermann, J. Jimenez, D. Harter, M. Dagenais, S. Fox, and Y. Hu, "Nonlinearly limited saturable-absorber mode locking of an erbium fiber laser," Opt. Lett. **24**, 1074–6 (1999).
6. K. Kieu, and F.W. Wise, "Soliton thulium-doped fiber laser with carbon nanotube saturable absorber," IEEE Photonics Technol. Lett. **21,** 128–130 (2009).
7. Y. Fedoryshin, P. Ma, J. Faist, P. Kaspar, R. Kappeler, M. Beck, J. F. Holzman, and H. Jäckel "Three operation modes for Tb/s all-optical switching with intersubband transitions in InGaAs/AlAs/AlAsSb quantum wells," IEEE J. Quant. Electron, **48**(7), 885–890 (2012).
8. Z. Sun, T. Hasan, F. Torrisi, D. Popa, G. Privitera, F. Wang, F. Bonaccorso, D. M. Basko, and A. C. Ferrari, "Graphene mode-locked ultrafast laser," ACS Nano **4**, 803–810 (2010).
9. H. Zhang, D. Tang, R. J. Knize, L. Zhao, Q. Bao, and K. P. Loh, "Graphene mode locked, wavelength-tunable, dissipative soliton fiber laser," Appl. Phys. Lett. **96** (2010).
10. S. Y. Set, H. Yaguchi, Y. Tanaka, and M. Jablonski, "Laser mode locking using a saturable absorber incorporating carbon nanotubes," Journal of Lightwave Technology **22**, 51–56 (2004).
11. F. Shohda, T. Shirato, M. Nakazawa, K. Komatsu, and T. Kaino, "A passively mode-locked femtosecond soliton fiber laser at 1.5 μm with a CNT-doped polycarbonate saturable absorber," Opt. Express **16,** 21191–21198 (2008).
12. D. Popa, Z. Sun, T. Hasan, W. B. Cho, F. Wang, F. Torrisi, and A. C. Ferrari, "74-fs nanotube-mode-locked fiber laser," Appl. Phys. Lett. **101**, (2012).
13. Z. C. Luo, M. Liu, H. Liu, X. W. Zheng, A. P. Luo, C. J. Zhao, H. Zhang, S. C. Wen, and W. C. Xu, "2 GHz passively harmonic mode-locked fiber laser by a microfiber-based topological insulator saturable absorber," Opt. Lett. **38,** 5212–5 (2013).
14. F. Shohda, M. Nakazawa, R. Akimoto, and H. Ishikawa, "An 88 fs fiber soliton laser using a quantum well saturable absorber with an ultrafast intersubband transition," Opt. Express **17,** 22499–22504 (2009).
15. F. B. Naranjo, P. K. Kandaswamy, S. Valdueza-Felip, V. Calvo, M. González-Herráez, S. Martín-López, P. Corredera, J. A. Méndez, G. R. Mutta, B. Lacroix, and E. Monroy, "Nonlinear absorption of InN/InGaN

multiple-quantum-well structures at optical telecommunication wavelengths," Appl. Phys. Lett. **98,** 031902 (2011).
16. F. B. Naranjo, M. Gonzáñez-Herráez, H. Fernández, J. Solís, and E. Monroy, "Third order nonlinear susceptibility of InN at near band-gap wavelengths," Appl. Phys. Lett. **90,** 091903 (2007).
17. L. Monteagudo-Lerma, S. Valdueza-Felip, F. B. Naranjo, P. Corredera, L. Rapenne, E. Sarigiannidou, G. Strasser, E. Monroy, and M. González-Herráez, "Waveguide saturable absorbers at 155 μm based on intraband transitions in GaN/AlN QDs," Opt. Express **21,** 27578 (2013).
18. Y. Li, A. Bhattacharyya, C. Thomidis, T. D. Moustakas, and R. Paiella, "Nonlinear optical waveguides based on near-infrared intersubband transitions in GaN/AlN quantum wells," Opt. Express **15,** 5860–5865 (2007).
19. S. C. Jain, and M. Willander, "III–nitrides: Growth, characterization, and properties," J. Appl. Phys. **87,** 965–1006 (2000).
20. J. Wu, "When group-III nitrides go infrared: New properties and perspectives," Journal of Applied Physics **106**, 1–28 (2009).
21. M. Akhmediev, J.M. Soto-Crespo, and P. Grelu, "Roadmap to ultra-short record high-energy pulses out of laser oscillators," Phys. Lett. Sect. A Gen. At. Solid State Phys. **372,** 3124–3128 (2008).
22. J. Koester, and E. Snitzer, "Amplification in a fiber laser," Appl. Optics, **3**(10), 1182 (1964).
23. J. Limpert, F. Roser, T. Schreiber, and A. Tünnermann, "High-power ultrafast fiber laser systems," IEEE J. Sel. Top. Quantum Electron. **12**, 233-244 (2006).
24. J. Tauc, "Optical properties and electronic structure of amorphous Ge and Si," Mater. Res. Bull. **3,** 37–46 (1968).
25. M. Haiml, R. Grange, and U. Keller, "Optical characterization of semiconductor saturable absorbers," Appl. Phys. B, **79**(3), 331-339 (2004).
26. I. D. Jung, F. X. Kärtner, N. Matuschek, D. H. Sutter, F. Morier-Genoud, Z. Shi, V. Scheuer, M. Tilsch, T. Tschudi, and U. Keller, "Semiconductor saturable absorber mirrors supporting sub-10-fs pulses," Appl. Phys. B Lasers Opt. **65,** 137–150 (1997).
27. S. Yamashita,, A. Martinez, and B. Xu, "Short pulse fiber lasers mode-locked by carbon nanotubes and graphene," Opt. Fiber Technol. **20,** 702–713 (2014).
28. S. Valdueza-Felip, L. Rigutti, F. B. Naranjo, P. Ruterana, J. Mangeney, F. H. Julien, M. González-Herráez, and E. Monroy, "Carrier localization in InN/InGaN multiple-quantum wells with high In-content," Appl. Phys. Lett. **101,** 1–5 (2012).
29. E. Snitzer, H. Po, R. Tumminelli, and B. C. McCollum, "Double clad, offset core Nd fiber laser," Opt. Fiber Sensors **2,** PD5 (1988).
30. L. Zenteno, "High-power double-clad fiber lasers," J. Light. Technol. **11,** 1435–1446 (1993).
31. L. Goldberg, B. Cole, and E. Snitzer, "V-groove side-pumped 1.5 μm fibre amplifier," Electron. Lett. **33,** 2127–2129 (1997).
32. F. X. Kartner, J. A. der Au, and U. Keller, "Mode-locking with slow and fast saturable absorbers-what's the difference?," IEEE J. Sel. Top. Quantum Electron. **4,** 159–168 (1998).
33. C. J. Chen, P. K. Wai, and C. R. Menyuk, "Soliton fiber ring laser," Opt. Lett. **17,** 417–9 (1992).
34. L. F. Mollenauer, and R. H. Stolen, "The soliton laser," Opt. Lett. **9,** 13–15 (1984).
35. J. D. Kafka, T. Baer and D. W. Hall, "Mode-locked erbium-doped fiber laser with soliton pulse shaping," Opt. Lett. **14,** 1269–1271 (1989).
36. B. Grudinin, and S. Gray, "Passive harmonic mode locking in soliton fiber lasers," J. Opt. Soc. Am. B **14,** 144 (1997).
37. R. Goldhahn, P. Schley, A. T. Winzer, G. Gobsch, V. Cimalla, O. Ambacher, M. Rakel, C. Cobet, N. Esser, H. Lu, and W. J. Schaff, "Detailed analysis of the dielectric function for wurtzite InN and In-rich InAlN alloys," Phys. Status Solidi Appl. Mater. Sci. **203**, 42–49 (2006).
38. S. Chouli, J. M. Soto-Crespo, and P. Grelu, "Optical spectra beyond the amplifier bandwidth limitation in dispersion-managed mode-locked fiber lasers," Opt. Express **19,** 2959–64 (2011).
39. M. Hofer, M. H. Ober, F. Haberl, M. E. Fermann, "Characterization of ultrashort pulse formation in passively mode-locked fiber lasers," IEEE J. Quantum Electron. **28,** 720–728 (1992).
40. K. Tamura, H. A. Haus, and E. P. Ippen, "Self-starting additive pulse mode-locked erbium fibre ring laser," Electron. Lett. **28,** 2226 (1992).
41. V. J. Matsas, T. P. Newson, and M. N. Zervas, "Self-starting passively mode-locked fibre ring laser exploiting nonlinear polarisation switching," Opt. Commun. **92,** 61–66 (1992).
42. F. Bonaccorso, Z. Sun, T. Hasan, and A. C. Ferrari, "Graphene photonics and optoelectronics," Nat. Photonics **4,** 611–622 (2010).

1. Introduction

Ultrafast mode-locked fiber lasers are the keystone in many fields of application such as telecommunications, industrial, medical processes and scientific research [1, 2]. These lasers combine a simple fabrication process with the capability to achieve extremely short pulses with moderately high peak power. The fiber ring configuration is the simplest way to achieve self-

starting mode-locking [2, 3]. Ultrafast mode-locked fiber lasers operating in the C-band (1.53 - 1.57 μm) have been developed since the introduction of the Er-doped fiber amplifier (EDFA) [4]. In this sources, passive mode-locking is achieved by insertion of a saturable absorber [5, 6], which typically consists of InGaAs/GaAsSb [7], and more recently of graphene [8, 9], carbon nanotubes [10–12], or CdS/ZnSe/BeTe [13, 14]. However, such materials have shown limited power range of operation, with average power typically in the milliwatt range or below.

III-nitride semiconductors can behave as saturable absorbers within the C-band involving either interband (bulk InN [15, 16], InN/InGaN quantum wells [15]) or intersubband transitions (GaN/AlN quantum wells or quantum dots [17, 18]). III-nitrides present not only high thermal and chemical stability, but also enhanced nonlinearities due to the asymmetry of their crystalline structure [19, 20]. However, the application of these materials to the development of ultrafast fiber lasers at telecom wavelengths has not been explored so far, to the best of our knowledge.

In this work, we demonstrate an ultrafast passively mode-locked and non-polarization-dependent fiber laser using InN as saturable absorber, operating at 1.55 μm. The laser shows pulsed emission with a repetition rate of 4.84 MHz and pulse width in the range of 240 - 260 fs, leading to peak power in the order of 4.7 - 8.0 kW. More importantly, the average output power is tunable over a range of ~100% without major variations in its performance.

In order to enhance the pulse peak power in the femtosecond range [21], the laser output is amplified using a master oscillator power fiber amplifier configuration (also known as MOPA, MOFA or MOPFA)[21–23]. This all-fiber configuration leads to pulses with time width below 55 fs and average output power about 250 mW, corresponding to peak power close to 1 MW.

2. Materials and methods

The saturable absorber consists of a 1-μm-thick In-polar InN layer grown by plasma-assisted molecular beam epitaxy (PAMBE) on a commercial 10-μm-thick non-intentionally doped GaN-on-sapphire template. The epitaxial process proceeded at a substrate temperature of 450 °C with a nitrogen-limited growth rate of 280 nm/h (more details can be found in [15], F.B. Naranjo et al.).

The absorption coefficient as a function of wavelength, $\alpha(\lambda)$, is obtained from the transmittance spectrum, $T(\lambda)$, applying, $\alpha = -\ln[T(\lambda)]/l$ where l is the layer thickness. The energy band gap has been estimated following the Tauc's approximation [24], leading to a value of $E_{gap} = 0.8 \pm 0.1eV$ ($\lambda = 1.55\mu m$) [see Fig. 1(a)]. Correcting reflection and scattering loses, the absorption coefficient of the InN layer at 1.55 μm is $\alpha(1.55\mu m) = 1.2 \times 10^4 cm^{-1}$.

Figure 1(b) shows the transmittance of the InN layer (T) as a function of the impinging laser fluence. A 1.55 μm ultrafast fiber laser (pulse width ~200 fs, temporal pulse spacing = 185 ns, maximum average power = 30 mW) has been used as the pump source, focused onto the InN sample using a 3-cm-focal achromatic lens. The setup induces a laser beam waist $\omega_0 \approx 12\mu m$ with a Rayleigh length $z_0 \approx 285\mu m$. The transmitted light is collected by a Ge detector connected to a multimeter (Agilent 34401A). The change in transmission can be described similarly as in [25], M. Haiml et al., but considering a transmittance configuration:

$$T = T_{ns} \frac{\ln\left(1 + T_{lin}/T_{ns}\left(e^{F/F_{sat}} - 1\right)\right)}{F/F_{sat}} \qquad (1)$$

where F is the impinging fluence, F_{sat} is the saturation fluence of the material, and T_{lin} and T_{ns} are the linear and non-saturable transmittance, respectively [25,26]. By fitting Eq. (1) to the

experimental measurements, we obtain $F_{sat} = 690 \pm 50 \mu J / cm^2$ (i.e. $I_{sat} \approx 3.4 GW / cm^2$), $T_{lin} = 28 \pm 1\%$, $T_{ns} = 53 \pm 1\%$. These values point to a highly nonlinear absorption (large modulation depth) in a material that stands extremely high fluencies (>5000 μJ/cm^2, which corresponds to a peak power of 35 GW/cm^2, the maximum achievable by our system) with no apparent damage. It must be noticed that the given values came from the fitting of Eq. (1) to the experimental data, which does not reach the maximum absorption saturation of the sample, leading to an underestimation of the calculated saturation fluence and non-saturable losses values. It should be noted the absence of reverse saturation of the absorption in Fig. 1(b). The obtained values are well above those of optimized nanostructures based on InGaAs quantum wells ($I_{sat} = 0.6 GW / cm^2$, damage threshold at 8 GW/cm^2) [7], graphene ($I_{sat} \approx 0.1 - 0.5 GW / cm^2$, damage threshold at 2 GW/cm^2) [27], and carbon nanotubes ($I_{sat} \approx 0.05 GW / cm^2$, damage threshold at 50 KW/cm^2) [27] as saturable absorbers at 1.5 μm. Furthermore, a relaxation time $\tau \approx 10\, ps$ has been measured in this material using the pump-and-probe technique [28]. This result is significantly slower than the relaxation time in InGaAs-based and graphene materials (below 1 ps [7, 27]).

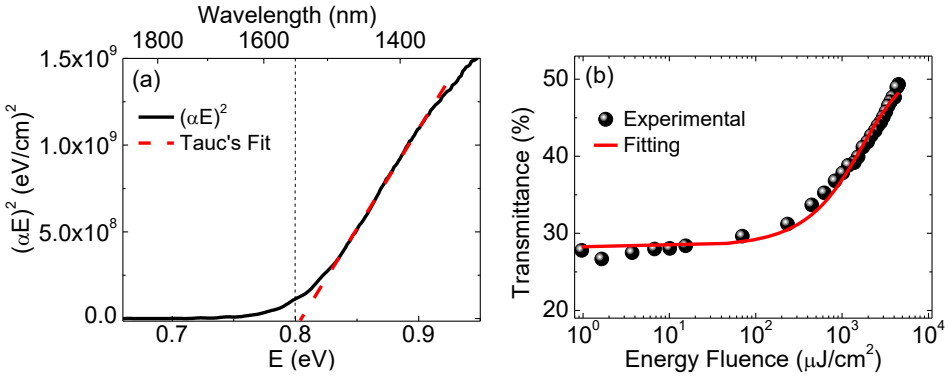

Fig. 1. Characterization of a 1-μm-thick InN layer: (a) Tauc's plot, i.e. $(E\alpha)^2$ vs. E, with E = energy, α = absorption coefficient. The dashed line is a linear fit for the determination of the band gap. The vertical dotted line marks the operation wavelength of the laser. (b) Variation of the optical transmittance as a function of the impinging energy fluence. The solid line is a fit of the experimental data to Eq. (1).

The InN saturable absorber is introduced within a fiber ring laser cavity, as shown in Fig. 2, at the focus of a system of two achromatic lenses with 3-cm focal length. A collimator lens has been used to launch the light from the optical fiber onto the first achromatic lens and a microscope objective to collect the light from the second lens into the fiber. A commercial EDFA (Accelink TV-Series) with a maximum output optical power of +24 dBm acts as the gain medium. A variable optical attenuator is used to control the optical losses within the cavity. A 90/10 optical fiber coupler recirculates 90% of the signal inside the cavity while the remaining 10% is driven to the laser output. The total length of the cavity was approximately 43 m, 16 m of which were Er-doped fiber with a normal group velocity dispersion GVD = 0.016 ps^2/m. The rest of the cavity length came from the pigtails of the used components, and was essentially single-mode fiber (SMF) with GVD = -0.021 ps^2/m. The laser has an estimated dispersion of –0.31 ps^2, i.e. the laser is operating at anomalous dispersion. Figure 3(a) depicts the peak power (in pulsed operation) as a function of the average output power for the different laser output regimes attained by varying the optical losses within the fiber ring with a variable

optical attenuator, namely continuous wave (CW), a transition range with the simultaneous emission of both CW and mode-locked components, and mode-locked. The normalized laser spectrum around 1.56 μm is depicted in Fig. 3(a) as an inset for each of the three regimes, showing the expected spectral broadening under mode-locked operation (the abscise span is the same, 100 nm for the three spectra). The laser is self-starting at a threshold power P_{out} ~ 5.5 mW. The inset of Fig. 3(b) shows the electrical spectrum during mode-locked operation, which displays a stable train of pulses with a repetition rate of ~ 4.84 MHz. It has been verified that the pulse train maintains stable amplitude in the whole mode-locked regime. No multiple-pulse behavior is observed in all the power range studied.

The repetition rate has been measured with a 20-GHz detector connected to an electrical spectrum analyzer with 32 GHz bandwidth (Agilent Technologies N9010A). The average power of the laser has been measured with an InGaAs power meter. The laser spectrum was recorded by connecting the 1% branch of the 99/1 fiber coupler to an optical spectrum analyzer (Yokogawa AQ-6315B) with a resolution of 0.5 nm. Autocorrelation traces are measured using the 500 fs scan range from a commercial autocorrelator (APE-Mini). To vary the cavity length, three SMF-28 optical fiber rolls with different nominal lengths (30 m, 45 m, 200 m) were used. The second EDFA used for the MOPA had double-cladding fiber [29, 30] and v-groove side pumping [31] in order to obtain high energy pulses. The maximum average output power is 40 dBm and including input and output single-mode fibers, it exhibits slightly anomalous dispersion (Keopsys KPS-BT2-C).

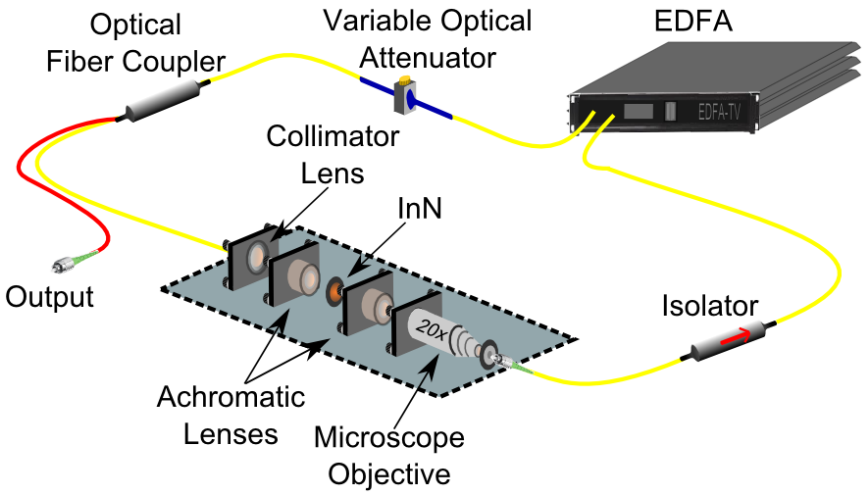

Fig. 2. Scheme of the C-band ultrafast mode-locked fiber laser using InN as saturable absorber.

3. Results and discussion

For the minimum attenuation, we obtain pulses with a temporal full width at half maximum (FWHM) $\Delta\tau = 252 \pm 4\, fs$ [see Fig. 3(b)]. At the same time, a spectral peak centered at $\lambda_c = 1563nm$ with spectral width $\Delta\lambda = 16.1 \pm 0.5nm$ is measured [see Fig. 3(c)]. Tuning the variable optical attenuator from the minimum attenuation [see Figs. 3(b) and 3(c)] to the mode-locked threshold [see Fig. 3(a)] results in a variation of the spectral width in the range from 17.1 ± 0.5 nm to 15.2 ± 0.5 nm, with pulse width varying from 258 ± 4 fs to 239 ± 4 fs. From these values, the calculated peak power [right axis of Fig. 3(a)] varies from 7.95 kW to 4.75 kW, respectively (pulse energy varying from 2 nJ to 1.13 nJ, respectively).

The spectrum and autocorrelation traces are well described by a hyperbolic-secant-squared function ($sech^2$) [see Figs. 3(b) and (c)]. This confirms the soliton nature of the pulse generation process [3, 32–36]. Solitons are nearly transform-limited pulses in which the pulse energy and duration are inversely related. In soliton lasers, very short pulses in the time domain (picoseconds to femtoseconds) are usually achieved, which leads to high peak energies. Figure 3(d) presents the Time-Bandwidth Product (TBP) for the previously described operation laser conditions. In the mode-locked range, the TBP is in the range of 0.32–0.35, close to the transform-limited value for $sech^2$ pulses (TBP = 0.315).

In the above-described laser, the InN saturable absorber is placed so that its <0001> crystallographic axis is aligned with the laser cavity. In such a configuration, the optical asymmetry within the basal plane of InN is too small [37] to induce remarkable changes with polarization of the incident light. Thus, the mode-locked threshold is independent of the laser polarization. This feature has been confirmed by introducing a polarization control element inside the cavity, which does not induce important changes in the emission properties of the laser for any polarization state.

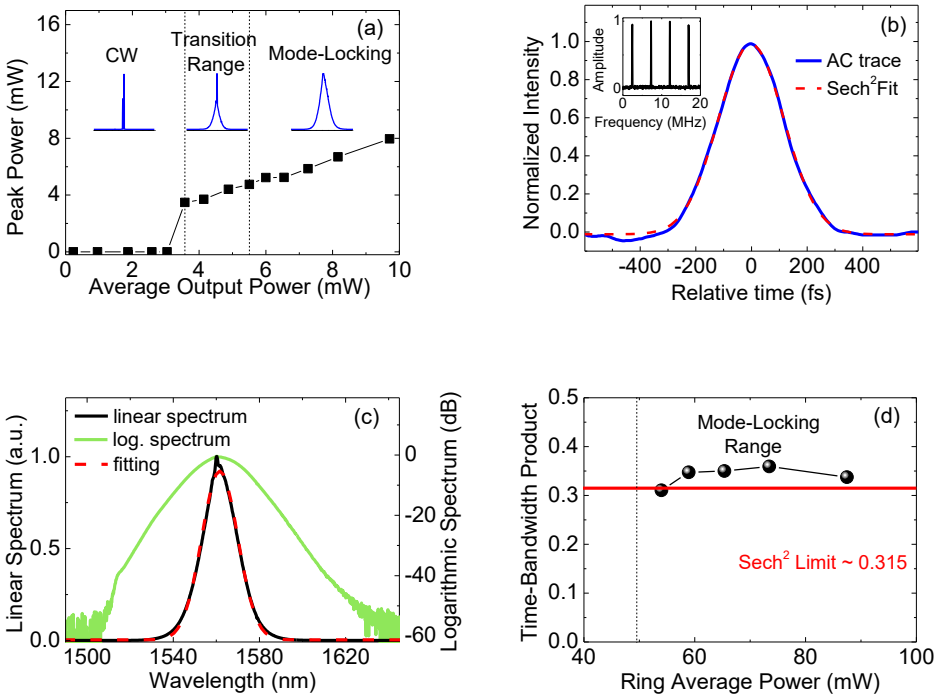

Fig. 3. Characterization of the fiber laser described in Fig. 2: (a) Variation of the peak power (only under pulsed operation, and zero in continuous wave) as a function of the average output power. The various operation regimes are identified: continuous wave (CW) and mode-locking (ML), with a ML lower threshold of 5.5 mW of average output power. The normalized linear spectra centered at 1.56 µm with a span of 100 nm are shown for each regime. (b) For the maximum ring average power (minimum attenuation in the ring, autocorrelation trace with a temporal duration of 252 fs. The inset shows the train of pulses generated with a repetition rate of 4.84 MHz. (c) Also for the maximum ring average power (minimum attenuation in the ring, laser spectrum centered at 1562 nm with a FWHM of 16 nm. (d) Time-Bandwidth Product as a function of the ring average power. The solid line represents the $sech^2$ limit.

It should be noted that, in our case, the laser is actually not a pure soliton laser but rather a dispersion-managed soliton laser (i.e. it has regions of normal and anomalous dispersion, and overall a low anomalous dispersion). In this type of laser, the pulse evolution along the cavity is breathing, meaning that it stretches and compresses temporally in each roundtrip as it passes through each sign of dispersion. The shortest achievable pulses in these fiber lasers occur when extracting the light in the single-mode fiber after the Er-doped fiber amplifier [38]. When these strongly chirped pulses with high power reach the single-mode fiber, self-phase modulation effect (SPM) becomes predominant, inducing a temporal compression, in our case leading to the measured ~250 fs FWHM. InN acts as a very efficient, slow saturable absorber, which leads to stable mode-locking with pulse duration well below its recovery time due to the formation of solitons, providing that the intracavity fluence is well above the saturation fluence of the absorber [32]. Considering that the distances between the optical coupler and the characterization systems (OSA, power meter, etc) and between the optical coupler and the saturable absorber are approximately the same (~2 m), we can expect that the pulse reaching the SA is as short as has been measured by the autocorrelator, but 9 times higher in average power, because of the optical coupler used. This assumption allows us to estimate the necessary fluence to reach the mode-locking threshold in $F = 6770 \mu J / cm^2$. Values of $\Delta\tau = 239 fs$ and $P_{out} = 5.5 mW$ (which implies an average power of 49.5 mW at the 90% branch of the fiber coupler) have been considered for this calculation. The maximum fluence handled by the saturable absorber in the developed laser system has been calculated in $F = 11940 \mu J / cm^2$, assuming $\Delta\tau = 252 fs$ and $P_{out} = 9.71 mW$ (which corresponds to an average power of 87.4 mW at the 90% branch of the fiber coupler). The high linear absorption coefficient, modulation depth and damage threshold of InN allow the generation of high-power pulses while keeping the CW laser emission blocked. The polarization independence is an advantage over those mode-locked fiber lasers whose principle of operation is based on a nonlinear-rotation-polarization acting as the saturable absorber, which need periodical readjustment of the polarization [39–41].

The study of the laser output properties for high pulse energy conditions is performed by inserting additional single-mode fiber between the output coupler and the variable attenuator (see Fig. 2), which leads to a reduction of the repetition rate. Figures 4(a) and 4(b) show the comparison between the autocorrelation traces and the spectra, respectively, for different additional fiber lengths up to 200 m, reaching a reduction of the repetition rate by a factor of 5, approximately [see Fig. 4(c)]. Table 1 summarizes the obtained results, showing negligible change in pulse duration, spectral width, and average power. This means that the peak power (P_p) and pulse energy (E_p) are multiplied by a factor of 5 simply by introducing 200 m of additional fiber to the standard configuration. It should be noted that the additional fiber also introduces a change in average dispersion, which could compensate the increase in pulse energy, thus maintaining the soliton pulse duration relatively stable. The maximum obtained pulse energy is Ep ~ 11 nJ, higher than the 7.3 nJ reported for a similar laser based on graphene [42]. Furthermore, the stability in pulse duration and spectral width implies that the TBP remains close to the transform-limited value for all these new configurations.

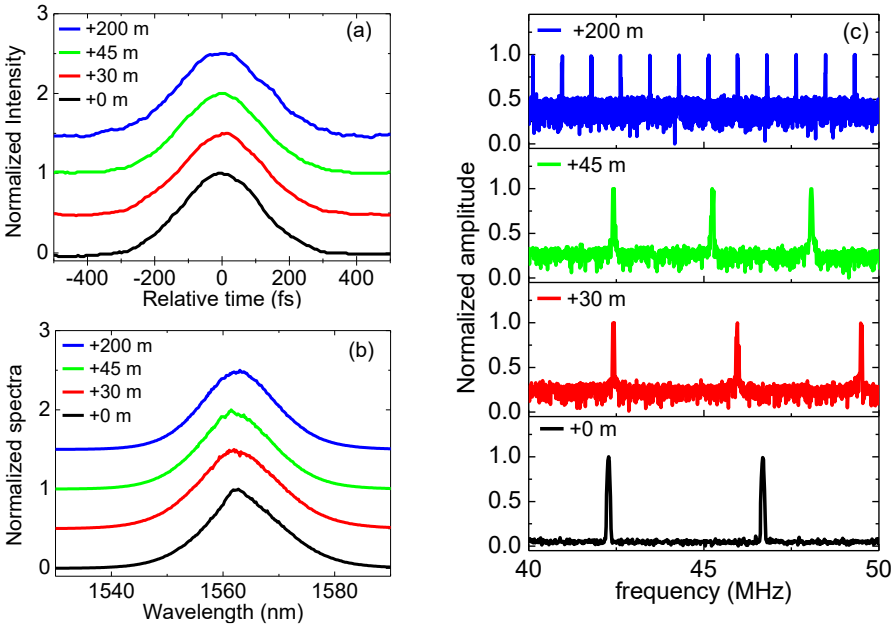

Fig. 4. Laser stability for different cavity lengths (from the standard configuration to +200 m of additional fiber): (a) autocorrelation traces (vertically shifted for clarity), (b) normalized spectra (vertically shifted for clarity), and (c) repetition rates.

Table 1. Experimental results comparing different laser cavity configurations differing in the length of an additional monomode fiber inserted between the output coupler and the variable attenuator (see Fig. 2).

Additional fiber length	+ 0 m	+ 30 m	+ 45 m	+ 200 m
Average Power (mW)	9.7	9.7	9.7	9.6
Repetition Rate (MHz)	4.84	3.54	2.84	0.84
$\Delta\tau$ (fs)	253 ± 4	265 ± 4	274 ± 4	277 ± 4
P_p (kW)	7.9	10.3	12.5	25.7
E_p (nJ)	2.0	2.7	3.4	11.4
TBP	0.34	0.38	0.36	0.36

In order to investigate the maximum achievable peak power, the laser output is amplified using a MOPA configuration. A second EDFA (see materials and methods section for more information) is connected to the output of the master oscillator while maintaining the original laser ring cavity. Figures 5(a) and 5(b) show spectra and autocorrelation traces, respectively, for different analyzed cases, maintaining the operation point of the master oscillator near the threshold. By changing the gain of the additional amplifier, the average output power can be tuned up to 358 mW, keeping the maximum of the emission spectra around 1575 nm. It is clearly visible the appearance of side-lobes when increasing the power. Since the appearance of these side-lobes, the pulse powers of Fig. 5(b) have been calculated by integrating the actual energy in the central peak. It has been estimated that only approximately 50% of the whole pulse energy remains in the central peak for the case of maximum average power (358 mW),

and 60% for the case when average power is $P_{av} = 224mW$. Figure 5(b) depicts pulse widths ranging from 65 $\pm$ 4 fs to 53 $\pm$ 4 fs. This temporal compression of the pulses results in pulse peak power varying from 0.42 MW to 0.7 MW. The temporal pulse compression is attributed to self-phase modulation (SPM) in the output amplifier (causing spectral broadening), followed by a subsequent compression in the anomalously dispersive output fiber. Figures 5(a) and 5(b) also show the spectrum and autocorrelation trace, respectively, for the particular case when the output amplification is minimum and the variable attenuator inside the ring laser cavity is totally open (mode-locking far from the threshold). The measured spectrum is shifted to larger wavelengths (up to 1633 nm). This redshift of the emission is attributed to Raman self-frequency shift due to stimulated Raman scattering in the output amplifier. In these conditions, the measured output average power is 207 mW and the pulse width is $120 \pm 4\,fs$, which implies that the peak power reaches 358 kW. Further increasing the power by output amplification leads to the appearance of side-lobes around the central emission peak, evidencing the increasing effect of SPM.

The introduction of the described amplification stage after the mode-locked fiber oscillator (MOPA) leads to additional temporal compression of pulses, which in turn results in an additional enhancement of the peak power. Figure 5(b) illustrates the appearance of pulse degradation and side-lobes when applying higher amplification. These are signatures of pulse break-up and initial stages of supercontinuum generation. For this reason, the output amplification has been limited in this work to values corresponding to high-quality pulses [23]. It should be noted, that in our case the soliton is propagating through an Er-doped amplifier acts as gain medium. The gain of the amplifier is bounded to approximately 1585-1590 nm. Thus, the spectra are somewhat clipped from this wavelength onwards. This distortion in the spectrum leads to a laser spectrum shape far from the pure sech^2 function, as it is shown in Fig. 5(a).

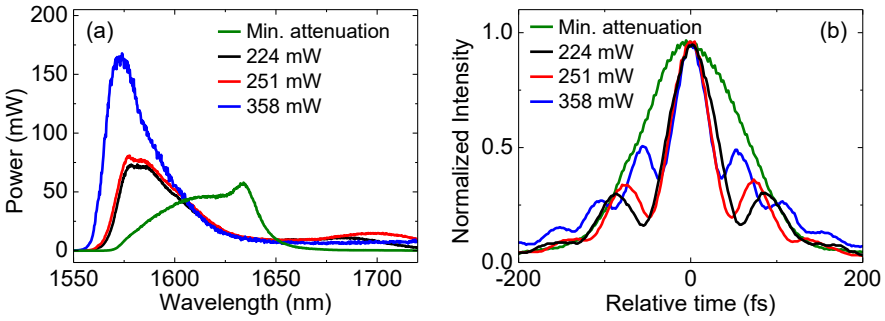

Fig. 5. Ultrafast mode-locked fiber oscillator using InN saturable absorber with output fiber gain: (a) spectra, and (b) autocorrelation traces for different amplification values operating close to the oscillator threshold, with master oscillator output average power of 5.5 mW. The legend indicates the average output power in each case. The green line corresponds to the case of minimum oscillator attenuation, i.e. far from the threshold with master oscillator output average power of 9.7 mW, and minimum output amplification (P_{Av}=207 mW).

4. Conclusions

In summary, this paper describes the first implementation of an ultrafast mode-locked fiber laser working at ~1.5 μm using InN as saturable absorber, which leads to an enhancement of the peak power and enlargement of the operation power range. This breakthrough is supported by the high energy fluence that InN can afford ($F > 11mJ / cm^2$) without any sign of optical

damage. Its high nonlinearity, along with the high stability of the InN response even for high pumping intensity, allows its use as efficient saturable absorber. The use of this saturable absorber within the resonator allows a large tunability in output power while preserving the output pulse properties. For a wide range of output powers, the pulses present no major changes in both spectrum and autocorrelation trace. This characteristic allows to overcome practical limitations shown by other fiber lasers operating at the same wavelength that use graphene [8], carbon nanotubes [10], InGaAs [7] or CdS/ZnSe/BeTe [14] as saturable absorbers. The simplicity of the InN layer used to mode-lock the laser and its high-tunable-power range of operation converts this laser in an appealing candidate for the immediate future of high power fiber lasers operating at telecom wavelengths. Furthermore, advantages over schemes based on Kerr-lens or nonlinear polarization rotation are evident, as no polarization sensitivity is noticed when using InN as saturable absorber. The laser configuration is therefore extremely robust against ambient fluctuations and mechanical variations.

Funding

Partial financial support was provided by the Spanish Government projects TEC2012-37958-C02-01 and TEC2015-71127-C2-2-R, the Community of Madrid project S2013/MIT 2790.

Acknowledgments

Authors want to thank Dr. J. Soto-Crespo for very fruitful discussions and Dr. S. Fernández for the transmittance measurements.